Accepted Manuscript

A new Schiff-base as fluorescent chemosensor for selective detection of Cr^{3+}: An experimental and theoretical study

Gholam Babaei Chalmardi, Mahmood Tajbakhsh, Nahid Hasani, Ahmadreza Bekhradnia

PII: S0040-4020(18)30311-9

DOI: 10.1016/j.tet.2018.03.046

Reference: TET 29386

To appear in: *Tetrahedron*

Received Date: 8 January 2018

Revised Date: 17 March 2018

Accepted Date: 21 March 2018

Please cite this article as: Chalmardi GB, Tajbakhsh M, Hasani N, Bekhradnia A, A new Schiff-base as fluorescent chemosensor for selective detection of Cr^{3+}: An experimental and theoretical study, *Tetrahedron* (2018), doi: 10.1016/j.tet.2018.03.046.

A new Schiff-base as fluorescent chemosensor for selective detection of Cr^{3+}: An experimental and theoretical study

Gholam Babaei Chalmardi[a], Mahmood Tajbakhsh[a]*, Nahid Hasani[a], Ahmadreza Bekhradnia[b*]

[a] Department of Organic Chemistry, Faculty of Chemistry, University of Mazandaran, Babolsar 47416-95447, Iran
[b] Pharmaceutical Sciences Research Center, Department of Medicinal Chemistry, Mazandaran University of Medical Sciences, Sari, Iran

E-mail: Mahmood.Tajbakhsh32@gmail.com, abekhradnia@gmail.com

Graphical Abstract

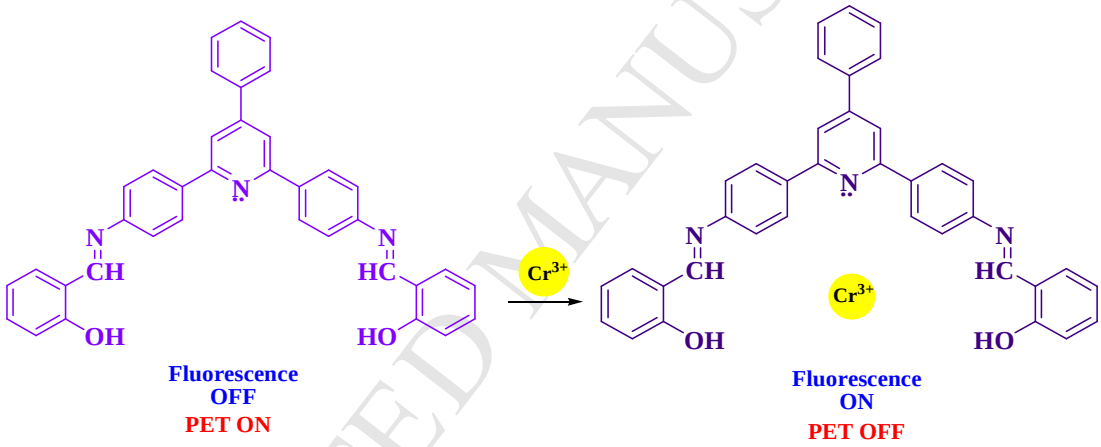

Highlights

· The Schiff base (**P3**) shows high selectivity towards Cr^{3+} ion compared with other competing metal ions.

· DFT calculations together with the experimental results obtained from Job's plot method showed a 1:1 binding ratio of Cr^{3+} with ligand **P3**.

· The sensing mechanism are explained by photoinduced electron transfer (PET) and chelation - enhanced fluorescence (CHEF).

· It has high affinity (K_a =2.28 × 10^5 M^{-1}) and selectivity for Cr^{3+}.

· The detection limit of the sensor towards Cr^{3+} is 1.3 × 10^{-7} M.

Abstract

A novel Schiff base fluorescent sensor N,N'-bis(salicylidene)-2,6-bis(4-aminophenyl)-4-phenylpyridine (**P3**) was synthesized through condensation of 2,6-bis(4-aminophenyl)-4-phenylpyridine and 2-hydroxybenzaldehyde. The obtained results from fluorescence analysis revealed that by excess of Cr^{3+} to **P3**, a remarkable increase was observed in the fluorescent intensity of the Schiff base at 663 nm with the ratio of CH_3CN/H_2O (95/5%), even though the other cations would likely have no impact on the fluorescence intensity. The cause of this trend might be ascribed to the formation of a 1:1 stoichiometric **P3**-Cr^{3+} complex, confirmed by Job's plot, which is resulted in preventing the photo-induced electron transfer (PET) process. From fluorescence titration, the association constant K_a was gained 2.28×10^5 M^{-1} and the limit of detection (LOD) was determined to be 1.3×10^{-7} M. Furthermore, the optimized structure together with the electronic spectra of the proposed complex was determined by DFT and TDDFT calculations.

Keywords: Fluorescence, Chemosensors, Schiff-base, PET, DFT, Chromium ion.

1. Introduction

The synthesis and development of new fluorescent chemosensors with the goal of detecting the heavy and transition metal ions are attractive and promising, whereas their use is growing fast in several research areas such as supramolecular chemistry, organic chemistry, drug delivery, biological chemistry and environmental chemistry [1–2]. Among these compounds, N-heterocycles are considerable attention toward chemosensors due to their high selectivity and sensitivity and also most important moieties in medicinal chemistry [3–5]. To tackle the environmental and medical challenges, a significant effort has been devoted in designing small-molecule florescent organic issues for chromium (Cr^{3+}) ion sensing. This vital ion, as an essential nutrient, plays a major role in the metabolism of carbohydrates, lipids, proteins, and nucleic acids in human body [6]. Another most important reason for enhancing the risk factors connected with diabetes and cardiovascular disease is concerned to insufficient dietary intake of chromium ion [7].

On the other hand, chromium is recognized as a noxious pollutant, omitted through various industrial and agricultural activities, that it can definitely be detrimental for both environment and human health. [8]. Despite the biological and environmental benefits of Cr^{3+}, few reports regarding fluorescent detection of Cr^{3+} are available [9-14]. A diversity of electron transition mechanisms, for example, chelation enhanced fluorescence (CHEF), intermolecular charge transfer (ICT), fluorescence resonance energy transfer (FRET), metal to ligand charge transfer (MLCT), photoinduced electron transfer (PET), photoinduced proton transfer (PPT), excited state intermolecular proton transfer (ESIPT), chelation-enhanced fluorescence (CHEF) effect, and C=N isomerization has been considered for developing fluorescent chemosensors [15–20]. Among the mentioned mechanisms, PET process has been used as a sensing tool in which the electron transfer directly occurs between the fluorophore (signaling unit) and the receptor ("switch" of the fluorescence intensity) [21–23]. The receptor unit can be connected chemically to fluorophore with absorption of shorter wavelength, where the PET efficiently happens between donor-acceptor probes [24–26]. In this regard, the electron-donating Schiff base ligand, can be considered as a receptor unit to absorb short wavelength light through forming chelate complex with the metal ions. Due to paramagnetic property of Cr^{3+} ion and the deficiency of a selective multi-chelating ligand, the appropriate fluorescent turn-on chemosensors to monitor intracellular Cr^{3+} are still under developed [27]. With this approach, we report a new chemosensor, N,N'-bis(salicylidene)-2,6-bis(4-aminophenyl)-4-phenylpyridine (**P3**) for Cr^{3+} that was prepared by condensing 2,6-bis(4-aminophenyl)-4-phenylpyridine with 2-hydroxybenzaldehyde (Scheme 1). Upon addition of Cr^{3+}, **P3** shows a large fluorescence enhancement because of the formation of a 1:1 **P3**-Cr^{3+} complex that inhibits photo-induced electron transfer (**PET**) process. The other metal ions including Na^{+}, K^{+}, Bi^{2+}, Hg^{2+}, Co^{2+}, Cu^{2+}, Zn^{2+}, Cd^{2+}, Fe^{3+} and Al^{3+} have almost no influence on the fluorescence.

To get more insight related to the electronic structures of **P3** and **P3**-Cr^{3+} complex, density functional theory (DFT) calculations were carried out on the plausible structures of the molecules. Moreover, time dependent density functional theory (TDDFT) was used as an accurate method for finding the excited state energies and UV-Vis absorption spectra of **P3** and **P3**-Cr^{3+} complex.

2. Experimental

2.1. General and reagents

Melting points were measured on an Electrothermal 9100 apparatus. Mass spectra were obtained on an Agilent 5975c spectrometer operating at 70 eV. ^{1}H and ^{13}C spectra were measured with Bruker DRX-400 AVANCE spectrometer at 400.1and 100.6 MHz, respectively. The UV-Vis spectra were recorded using a Perkin-Elmer lambda-EZ 201 and a Jasco FP-200 spectra fluorometer was used to obtain fluorescence emission spectra. Fluorescence intensity measurements were performed in CH_3CN/H_2O (95/5%) at room temperature.

2.2. Synthesis

2.2.1. Synthesis of 2,6-bis(4-nitrophenyl)-4-phenylpyridine (P1)

A mixture of benzaldehyde (6.4 g, 0.06 mol), p-nitroacetophenone (20 g, 0.12 mol), ammonium acetate (60 g), in glacial acetic acid (150 ml) was refluxed for 2 h [28]. After cooling the reaction mixture to room temperature a solid residue was obtained which then filtered and washed with acetic acid (50%) and cold ethanol, respectively. The crude 4-phenyl-2,6-bis(4-nitrophenyl) pyridine (*P1*) was recrystallized from absolute ethanol, and dried under vacuum (Scheme1). Yield: 66%, mp: 319-321 °C, ^{1}H NMR (400 MHz, $CDCl_3$), δ, ppm: 8.43-8.38 (8H, m), 8.07 (2H, S), 7.80-7.77 (m, 2H), 7.63-7.56 (3H, m). ^{13}C NMR (100 MHz, $CDCl_3$), δ, ppm: 155.52, 151.39, 148.44, 144.83, 137.90, 129.73, 129.42, 127.94, 127.19, 124.11 and 119.12 (Fig. S1).

2.2.2. Synthesis of 2,6-bis(4-aminophenyl)-4-phenylpyridine (P2)

A mixture of 4-phenyl-2,6-bis(4-nitrophenyl) pyridine (13.75 g, 48mmol) and palladium on carbon 5% (5 g) in ethanol (500 mL) as solvent were prepared in a two-necked round-bottomed flask (500 ml) equipped a dropping funnel. The mixture was warmed up to 50 ºC and then hydrazine hydrate 85% (35 ml) in ethanol (50 ml) was added dropwise over a 1.5 h period through the dropping funnel while maintaining the temperature at about 50 ºC. The reaction mixture was then refluxed for 2 h and filtered. Upon cooling, the filtrate gave white colored crystals of the *2,6-bis(4-aminophenyl)-4-phenylpyridine (P2)*, which were recrystallized from ethanol and vacuum dried. (Scheme1). Yield: 64%. mp: 207-209 °C. ^{1}H NMR (400 MHz, $CDCl_3$), δ, ppm: 8.068 (4H, d, J=8.4 Hz), 7.77-7.72 (4H, m), 7.54 (2H, T, J=7.6 Hz), 7.48(1H, d, J=7.2 Hz), 6.82 (4H, d, J=8.4 Hz), 3.85 (4H, S, NH_2). ^{13}C NMR (100 MHz, $CDCl_3$), δ, ppm:

157.13, 149.72, 147.32, 139.67, 130.30, 128.98, 128.65, 128.26, 127.16, 115.05 and 114.86 (Fig. S2).

2.2.3. N,N'-bis(salicylidene)-2,6-bis(4-aminophenyl)-4-phenylpyridine *(P3)*

A solution included 2-(6-(2-aminophenyl)-4-phenylpyridin-2-yl)benzenamine (1 mmol) in absolute ethanol was added to an ethanolic solution of 2-hydroxybenzaldehyde (2 mmol). The mixture was refluxed for 6 h and then cooled to room temperature. The solvent was evaporated to afford yellow product which was recrystallized from ethanol (Scheme1). Yield: 87%. mp: 189-193 °C. ^{1}H NMR (400 MHz, $CDCl_3$), δ, ppm: 13.29 (2H, S), 8.74 (2H, S), 8.32 (4H, d, J 8), 7.94 (2H, S), 7.79 (2H, d, J=7.2 Hz), 7.59-7.52 (3H, m), 7.47-7.41 (8H, m), 7.07 (2H, d, J=8 Hz), 7.01(2H, t, J=7.2 Hz). ^{13}C NMR (100 MHz, $CDCl_3$), δ, ppm: 162.75, 161.25, 156.69, 150.43, 149.15, 138.92, 138.08, 133.34, 132.41, 129.19, 129.13, 128.21, 127.21, 121.59, 119.25, 119.16, 117.33, and 117.03. The mass spectrum showed a peak at m/z = 545.2 corresponding to compound **P3** (Figs. S3 and S4).

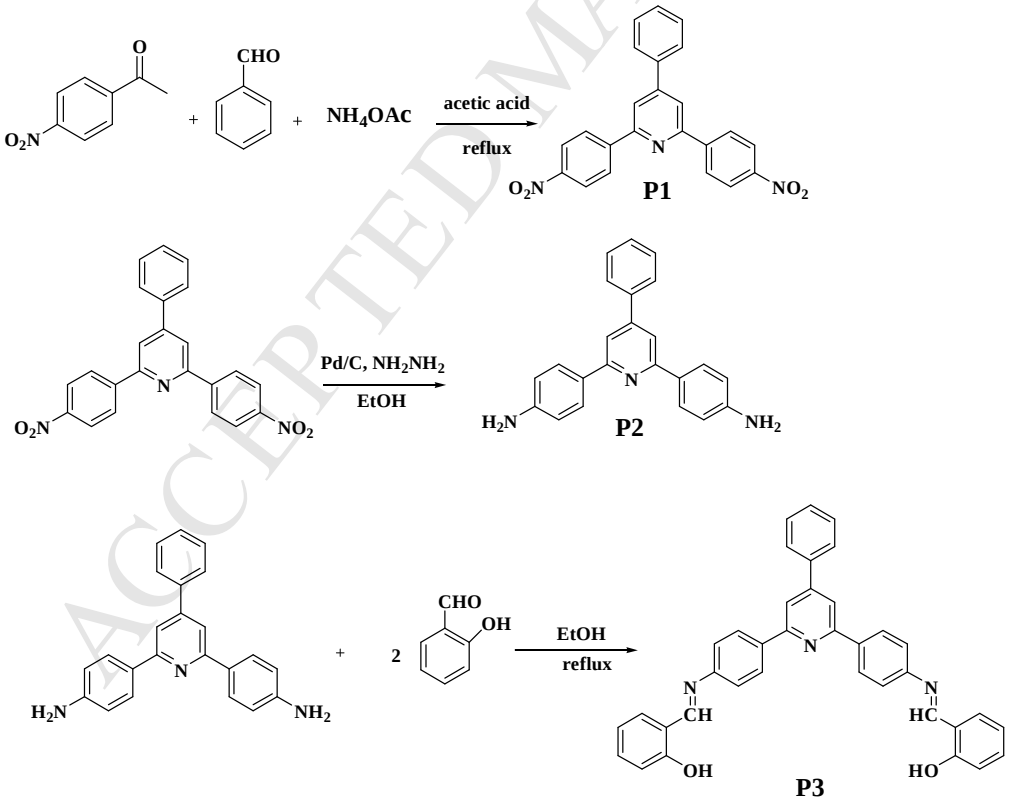

Scheme 1. The synthetic route of compound **P3**.

2.3. Spectrometric procedure

Stock solutions (10 μM) of nitrate salts of Na^{+}, K^{+}, Bi^{2+}, Hg^{2+}, Co^{2+}, Cu^{2+}, Zn^{2+}, Cr^{3+}, Cd^{2+}, Fe^{3+}, Al^{3+} in CH_3CN/H_2O (95/5%) were prepared and compound **P3** was dissolved in CH_3CN/H_2O (95/5%), (10 μM). Test solutions were prepared by placing 2 mL of the probe stock solution into cuvettes, adding 2mL of each metal ion stock. For all measurements, excitation wavelength was at 360 nm.

2.4. DFT procedure

The electronic structures of the titled compounds were optimized by density functional calculations (DFT) without any symmetry constraints, employing the Gaussian09 package [29]. Frequency calculations were performed on all the optimized geometries to ensure the correct local minima. Al the calculations were carried out in the framework of the Becke three-parameter hybrid exchange and Lee–Yang–Parr correlation functional (B3LYP) together with a split-valence Pople basis set plus polarization and diffuse functions, 6-31+G (d,p) for H, C, N, and O atoms and a double-ζ quality LANL2DZ basis set for Cr atom [30]. All the "inner electrons" of metal ions were replaced and described with a scalar relativistic electron core potential (ECP). Time-dependent density functional theory (TD-DFT) calculations were performed to attain the UV-Vis spectra and characterization of the frontier orbitals, at B3LYP/6-31+G (d,p) level with the polarized continuum model (IEFPCM) in acetonitrile solvent [31].

3. Results and discussion

3.1. Spectral studies

The outcomes obtained from absorption and fluorescence spectral analysis, upon addition of a variety of metal ions to **P3** solution with the ratio of CH_3CN/H_2O (95/5%) were shown in Fig.1 and Fig. S5. The absorption spectra of **P3** (10 μM) in CH_3CN/H_2O (95/5%) solution display three bands at 236 nm, 316 nm and 360 nm. After addition of various metal ions such as Cr^{3+}, Na^{+}, K^{+}, Bi^{2+}, Hg^{2+}, Co^{2+}, Cu^{2+}, Zn^{2+}, Cd^{2+}, $Fe^{3+}$and Al^{3+}, the absorption intensity of the peaks were decreased which can be attributed to the hypochromic effects in the UV-Vis spectra of **P3** (Fig. S5). It seems the UV-Vis spectra cannot be likely an alternative to demonstrate the specific sensitivity of **P3** to the cations due to the ambiguous absorption spectra within mixture species [32]. To this reason, the selectivity of **P3** towards Cr^{3+} among other metal ion solutions (10

µM) was investigated by fluorescence spectroscopy in CH_3CN/H_2O (95/5%) solution. As shown in Fig 1, the sensor **P3** without Cr^{3+} exhibits the weak fluorescence intensity with excitation at 363 nm. Upon addition of various metal ions, the Cr^{3+} has only displayed a considerably enhancement of fluorescence, which is indeed demonstrated the high selectivity of **P3** for Cr^{3+}. This could be assigned to the formation of a 1:1 stoichiometric **P3**-Cr^{3+} complex associated with the inhibiting of photo-induced electron transfer (PET) process [33-35].

a)

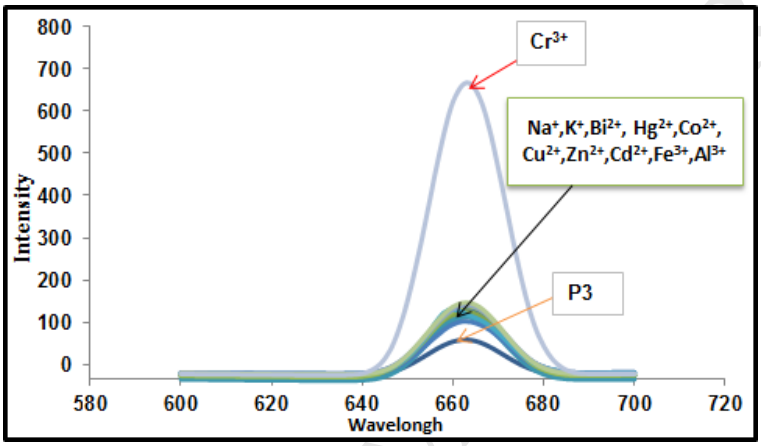

b)

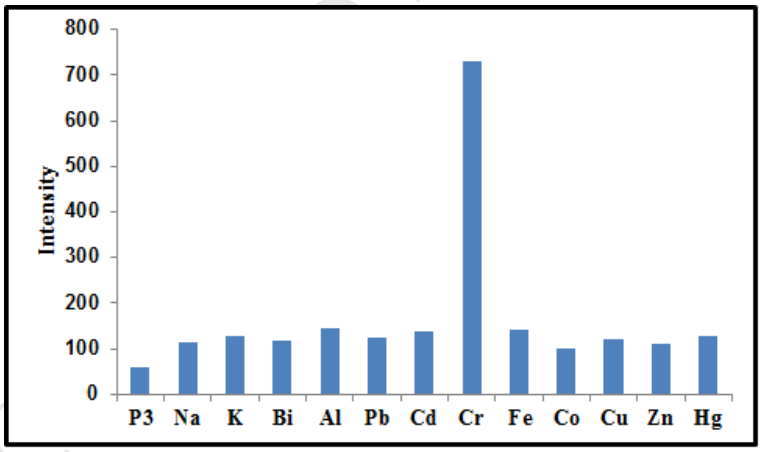

Fig. 1. (a) Fluorescence responses of compound **P3** (10 µM) in CH_3CN/H_2O (95/5%) solution upon the addition of various metal ions (λex =360 nm, 2 equiv). (b) Bar graph representing the change of the relative emission intensity of **P3** at 663 nm upon treatment with various metal ions (λex = 360 nm).

By considering the fact that the Schiff base **P3** is quite sensitive to Cr^{3+} rather than other metal ions, the absorption of ligand **P3** in a mixture of other metal ions in CH_3CN/H_2O (95/5%)

solution both in absence and presence of Cr^{3+} have been measured which resulted in observing a drastic enhancement in fluorescence intensity of (**P3**-other cations-Cr^{3+}) mixture than the another one (shown in Fig. 2). These observations can likely confirm the trend of **P3** as an efficient and selective fluorescence chemosensor for Cr^{3+} ion.

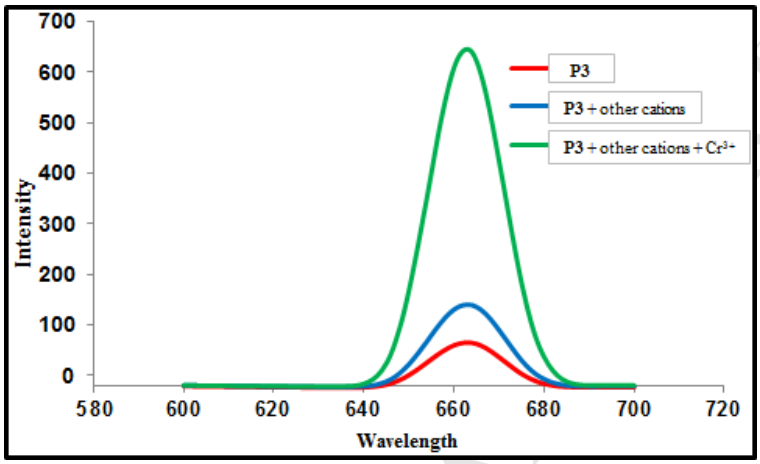

Fig. 2. Fluorescence intensity of **P3** (10 µM) in the absence of metal ions (red curve), and presence of 2 equiv of all kinds of competitive metal ions (blue curve) in CH_3CN/H_2O (95/5%, λex = 360 nm. The green curve represents the addition of Cr^{3+} to the above mixture. Each spectrum was acquired 1 minute after cations addition at room temperature.

In order to gain further insights concerning the chemosensing properties of receptor **P3**, a fluorescence titration of receptor **P3** with Cr^{3+} has been carried out. The results were in accordance with our claim so that by raising the concentration of Cr^{3+}, the sensitivity of **P3** towards Cr^{3+} ions was obviously increased as it is shown in Fig. 3. The fluorescence spectrum of **P3** (λ_{em} = 663 nm) shows the rapid turn-on responses and the inset is indication of the relative fluorescence intensity changes as a function of Cr^{3+} concentration.

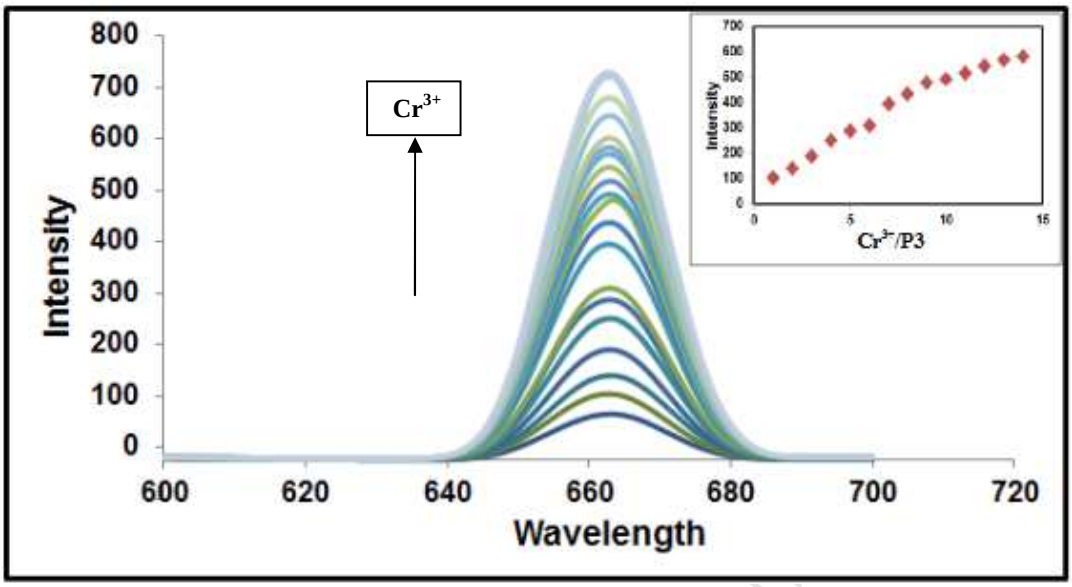

Fig.3. Fluorescence titration of **P3** (10 µM) with various concentration of Cr^{3+} in CH_3CN/H_2O (95/5%) solution (excitation = 360 nm) at room temperature. inset: changes of fluorescence upon addition of Cr^{3+} (0-2 equiv) at emission=663 nm.

Furthermore, the association constant (K_a) of binding of **P3** with metal ions was determined by Benesi–Hildebrand equation [36] as follows:

$$\frac{1}{F - F_0} = \frac{1}{K_a(F_{max} - F_0)[M]} + \frac{1}{F_{max} - F_0}$$

F and F_0 represent the fluorescent intensity of compound **P3** in the presence and absence of metal ions, respectively. F_{max} is the saturated fluorescent intensity of compound **P3** in the presence of excess amount of metal ions and [M] is the concentration of the added metal ions. The association constant of **P3**-Cr^{3+} complex was determined to be 2.28 × 105 M^{-1} using the results obtained from fluorescence titration. Moreover, the detection limit of **P3** was estimated based on the fluorescence titration while to gain the S/N ratio, the emission intensity of the complex (**P3**-Cr^{3+}) was calculated along with the standard deviation of blank measurements. Then, the detection limit for Cr^{3+}, according to $3 \times \delta_b/m$, was found to be 1.3×10^{-7} mol/L, where δ_b and m are the standard deviation of blank solutions and the slope between intensity versus sample concentration, respectively[37].

In alignment with our research studies, the fluorescence quantum yield for the **P3**-Cr^{3+} complex was determined through comparison of both emission and absorption intensities of the bands with those of a fluorescence standard (fluorescein in 0.1 N NaOH) [38] which was obtained to be 13.8%. For all the fluorescence measurements, the region of excitation was in 360 nm with slit widths of 3.0 nm. However, the negligible quantum yields calculated for combined receptor and the other cations as well as free receptor are not reported.

3.2. Binding mode studies

To find out the stoichiometry of binding between the receptor **P3** and Cr^{3+}, the Job's method of continuous variation was utilized. The total concentration of the complex **P3**-$Cr^{3+}$was constant (10 µM), with a continuous variable molar fraction of guest ([P3]/[Cr^{3+}] + [**P3**]). Fig. 4 shows the Job's plot of ligand **P3** with Cr^{3+} (at 663 nm) in which the fluorescence emission intensity indicates a maximum, whereas the molar fraction of **P3** is 0.5. As a result, a stoichiometry of 1:1 was confirmed for the complex Cr^{3+}-**P3**.

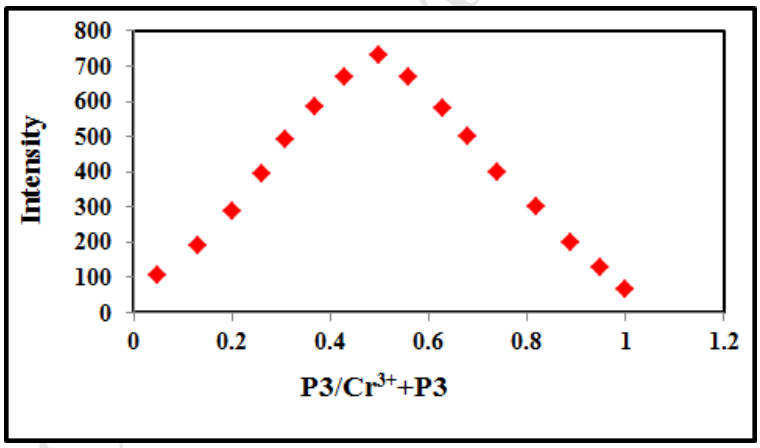

Fig. 4. Job's plot for determining the stoichiometric complexation of **P3** with Cr^{3+} in CH_3CN/H_2O (95/5%) at room temperature. The total concentration of **P3** and Cr^{3+} is 10 µM.

In addition, the ^1H NMR titration experiments were applied to support the binding of receptor **P3** to Cr^{3+} to form a metal complex. The experiment was conducted by addition of increasing concentrations of Cr^{3+} to the **P3** solution, so that the phenolic OH signals of **P3,** centered at 13.29 ppm, was disappeared after addition of 2 equivalent of Cr^{3+}. This implies that

the phenolic OH groups are vital to make a stable complex between the **P3** and Cr^{3+}. The binding mode of **P3** and Cr^{3+} is meaningful for the formation of novel Cr^{3+} fluorescent chemosensor [39, 40].

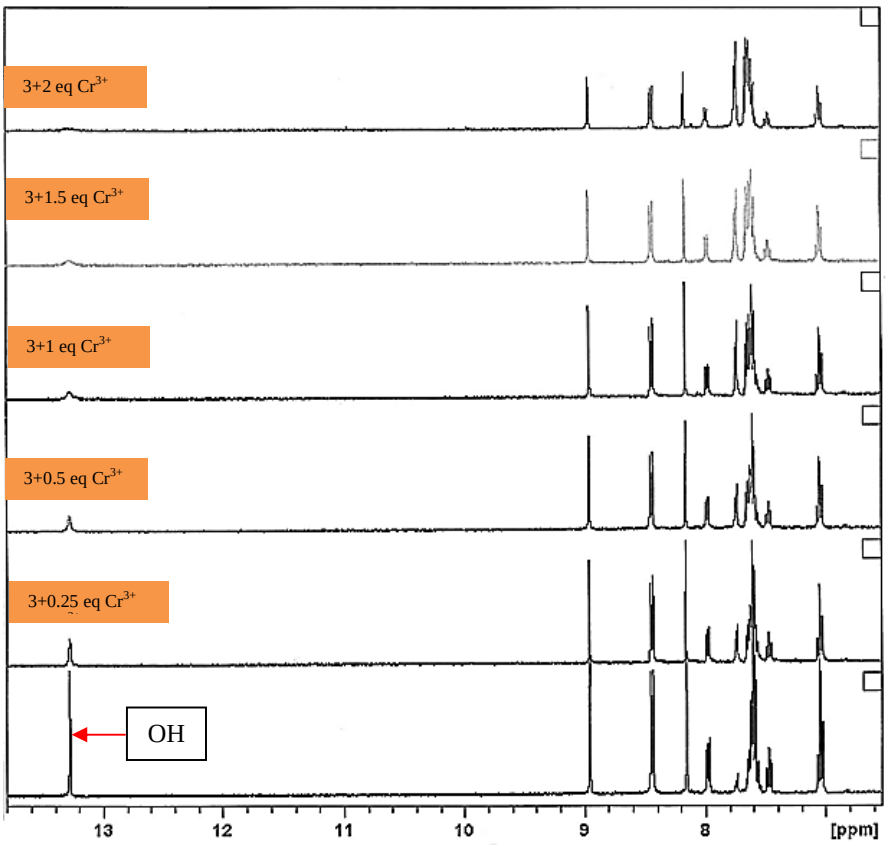

Fig. 5. Partial ^1H NMR spectra of **P3** (10 µM) in CD_3CN at room temperature and the corresponding changes after the addition of increasing amounts of Chromium nitrate (0-2 equiv). Each spectrum was acquired 1 minute after Cr^{3+} addition at room temperature.

3.4. Solvent effect

It is found that the character of optical sensing in the chemosensors is connected to the polarity of solvents. Hence in this study, the response of ligand **P3** to Cr^{3+} ion in various media such as DMSO, DMF, methanol, acetonitrile and acetonitrile/H_2O was investigated at maxima of emission intensity. The diagram (shown in Fig. 6) shows the optimum fluorescence emission occurs both in acetonitrile and acetonitrile/H_2O (95/5%) solvents. On the other hand, the aprotic (DMSO, DMF) and protic (methanol, H_2O) media results in a significantly reduction in fluorescent intensity These observations can be due to hydrogen bonding formation between

solvents and hydroxyl groups, rather than general solvent effects [41]. Nevertheless, the highest fluorescent intensity was observed in acetonitrile and acetonitrile/H_2O (95/5%), and hence the later was chosen as solvent [42].

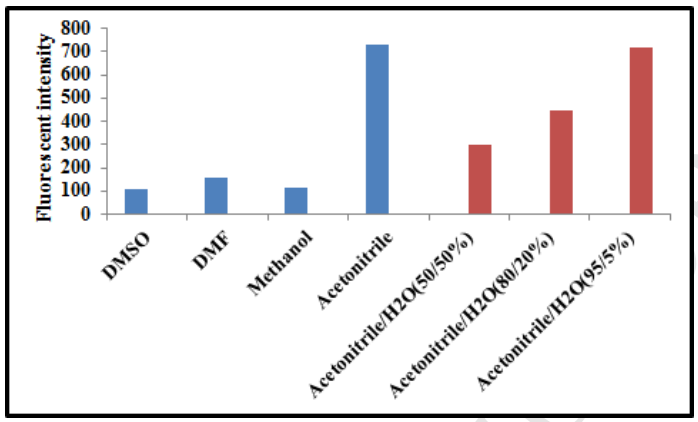

Fig. 6. Solvent effect on fluorescent intensity of **P3** (10 µM) with Cr^{3+} (2 equiv) in different solvent DMSO, DMF, methanol, acetonitrile, acetonitrile/H_2O (50/50%), acetonitrile/H2O (80/20%), acetonitrile/H2O (95/5%).

*3.5. Effect of pH on the binding affinity of Cr^{3+} to **P3***

Due to the critical role of the medium pH in the fluorescence detection of the chemosensors, in this study the effect of pH (in the range of 2 to13) on the fluorescence response of **P3** was investigated in CH_3CN/H_2O (95/5%) mixture. The changes in the fluorescence intensity at 663 nm of **P3** in both absence and presence of Cr^{3+} ion were plotted as a function of pH (Fig. 7). The overall intensity of **P3**–Cr^{3+} remained higher than the free receptor **P3**. Fluorescent intensity was found to be the highest at pH 9. For measurements outside the pH 9, Cr^{3+} might be appeared as $Cr(OH)_3$ species, removed from **P3**, thus the outcomes can be impacted on emission intensity as decreasing. In the same manner, below pH 9, **P3** might be combined with H^+ and show no tendency to bind Cr^{3+} resulting a decrease in the fluorescence intensity. So, **P3** can tolerate the detection of Cr^{3+} in the pH 9 [43].

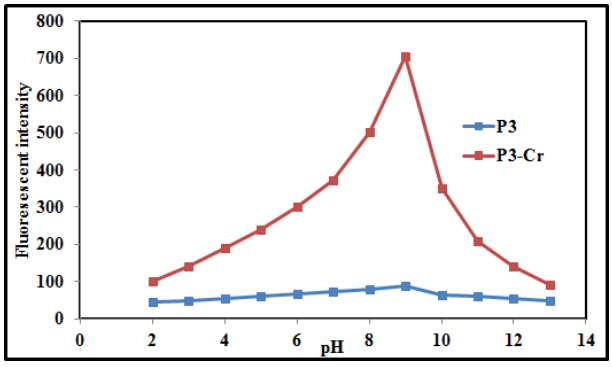

Fig. 7. Fluorescence response for **P3** in the absence and presence of Chromium as a function of pH in CH_3CN/H_2O (95/5%) at 663 nm.

3.6. Comparison

To find reliable results, the chemosensor **P3** was compared to those previously reported chemosensors for Cr^{3+} and the data are tabulated in Table 2. In comparing manner, the detection limit, binding constant, sensing response, and pH range exhibited that **P3** was efficient sensor in compare with other synthetic ionospheres [44-48] in table 2.

Table 2: Comparative analysis of chemosensor **P3** with previously reported sensors.

Ionophores	mechanism	Methods of detections	Medium of detection	Detection limit (M)	Binding Constant M^{-1}	Sensing response	pH range
Ref. 40	PET and CHEF	fluorescent	CH_3CN/H_2O (95/5%)	2.2×10^{-7}	8.77×10^{4}	Cr^{3+} (Turn on)	8
Ref. 44	-	fluorescent	CH_3CN/H_2O (8/2)	7.94×10^{-5}	1.6×10^{4}	Cr^{3+} (Turn on)	7
Ref. 45	PET	colorimetric and fluorescent	MeOH	1.21×10^{-6}	1.01×10^{4}	Cr^{3+} (Turn on)	2-7
Ref. 46	-	colorimetric and fluorescent	MeOH	1.1×10^{-5}	1.4×10^{4}	Cr^{3+} (Turn on)	-
Ref. 47	C=N isomerization and ESIPT	colorimetric and fluorescent	CH_3CN	2.75×10^{-6}	5.97×10^{4}	Cr^{3+} (Turn on)	-
Ref. 48	-	fluorescent	CH_3CN	9.86×10^{-6}	2.1×10^{3}	Cr^{3+} (Turn on)	6-8

P3	PET and CHEF	fluorescent	CH_3CN/H_2O (95/5%)	1.3×10^{-7}	2.28×10^5	Cr^{3+} (Turn on)	9

3.7. Theoretical study

3.7.1. The optimization calculations

The experimental results revealed that the Schiff base ligand (**P3**) is quite sensitive to Cr (III) ion compared to the other metal ions, nevertheless, the coordination geometry of the ligand to bind Cr(III) ion is still ambiguous. Since the crystal structures of **P3** ligand and **P3–Cr^{3+}** complex could not be determined by X-ray spectroscopy due to taken fine powders of the compounds. To this reason, plausible tetrahedron geometry of **P3–Cr^{3+}** complex was considered to the titled compound. The assuming structures of both of both **P3** and **P3–Cr^{3+}** compounds were optimized using DFT calculations at B3LYP/6-31G (d,p) levels of theory. The Optimized structures of **P3** and also **P3–Cr^{3+}** complex together with the selected calculated bond distances and angles are shown in Fig. 8 and Fig. 9, respectively. As shown in Fig. 8, the Schiff base (**P3**) behaves as a tridentate ligand that was coordinated through N atom of phenylpyridine (N1) and two oxygen atoms of salicylidene (O1 and O2) groups. So, the best possible structure of **P3–Cr^{3+}** complex results in a distorted tetrahedral coordination geometry in which one oxygen atom (O3) of nitrate group and also O1, O2 and N1 atoms of **P3** ligand could bind to Cr^{3+} ion, as is supported by the NMR spectra in experimental section (vide infra 3.2).

In order to investigate of binding mode of **P3** with Cr^{3+} ion, the ^1H NMR spectra of **P3** in the absence and presence of Cr^{3+} were investigated in CD_3CN (Fig. 5). The proton shift of **P3** at 8.74 ppm may be assigned to the proton of imine, which is fairly intact with addition of chromium ion to the **P3** solution. In spite of our previous study, N,N'-bis(salicylidene)-2,6-bis(2-aminophenyl)-4-phenylpyridine (**3**) [40] (Table 2), the results indicate that the proton of imine group is not involved in the formation of complex between the **P3** with Cr^{3+} ion. To attain a deeper insight, the evaluation was performed with the comparable studies. The comparison between **P3** and **3** [40] implied both fluorescent probes exhibit a fluorescence enhancement in the presence of Cr^{3+} through inhibition of photo-induced electron transfer (PET) mechanism.

In addition of Cr^{+3} ion, the fluorescent chemosensor of ligand **3** showed a single emission band at 537 nm upon excitation at 237 nm, whereas ligand **P3** revealed an outstanding increase in the fluorescent intensity at 663 nm upon excitation at 360 nm according to fluorescence emission studies. Also, the association constant (K_a) of binding of **P3**-Cr^{+3} was calculated around 10 times greater than **3-** Cr^{+3} by Benesi–Hildebrand equation.

A bond length increase of 0.029 Å for C2-C3 and 0.015 Å for C5-C6, from ligand to complex, lead to easier rotation of C-C groups. On the other hand, by decreasing the bond lengths of N2-C4 and N3-C1, the free rotation around of the complex is restricted which results in a tetrahedral geometry around the metal ion.

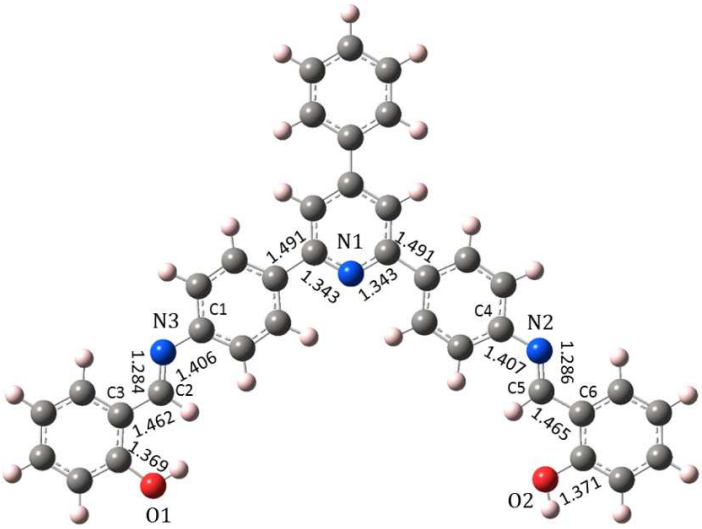

Fig. 8. Optimized geometry of the Schiff base ligand (**P3**) with B3LYP/6-31G(d, p) level.

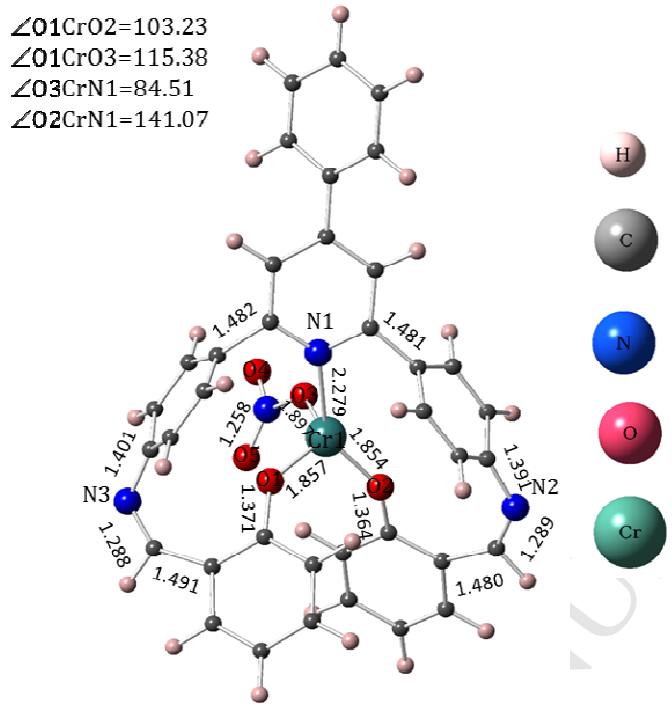

Fig. 9. Optimized geometries of **P3–Cr**$^{3+}$ complex with B3LYP/6-31G(d, p)/LANL2Z level.

3.7.2. The TDDFT calculations

The electronic spectra of both **P3** (Schiff base) and **P3**–Cr^{3+} complex, optimized with inclusion of acetonitrile solvent, were ascertained by TDDFT calculations to determine the energies and compositions of the molecular orbitals (MOs). The assignment of the most important occupied (HOMOs) and unoccupied (LUMOs) orbitals involved in electronic transitions in α and β spin states, with the fragment Mulliken contributions have been expressed in terms of the compositions from the central metal (Cr), (PhN) and (PhO) parts and also (Py) fragment (shown in Fig S6). The energy gap between HOMO and LUMO can be related to chemical activity of the molecules and tendency to intra. The TDDFT calculation revealed that upon coordination of ligand **P3** to Cr^{3+} ion, the energy levels of both the HOMO and LUMO slightly decreased relative to those of free **P3** (as shown in Fig. 10). Whereas, a small HOMO–LUMO energy gap favors electron hopping between both occupied and unoccupied molecular orbitals, the charge transfer in **P3**–Cr^{3+} complex would enhance, significantly than that for **P3** ligand [49-50]. The decrease of energy levels of LUMOs is more significant than those for the HOMOs ones, indicating that the LUMOs were considerably stabilized relative to the HOMOs. On the other hand, the conversion of **P3** to **P3**–Cr^{3+} complex becomes simple by narrowing the

energy gap between the HOMO and LUMO orbitals. So, it provides a reasonable explanation about that decrease of the energy gap of HOMO-LUMO from **P3** to its chromium complex (Fig. 10), which is in agreement with the subsequent generation of the new red shifted absorbance peak on the addition of Cr^{3+} to **P3** [50-51]. The formation of highly stable tetrahedron complex of **P3** with Cr^{3+} central metal, are resulted through the expansion of the conjugation of the aromatic groups and also an increase of charge transfer possibility, that caused to initiate this unusual fluorescence response. In addition, the theoretical calculations indicate that, in the **P3**–Cr^{3+} complex, the electron contributions in HOMO and HOMO-1 orbitals mainly were distributed over the donor part, namely PhN and PhO fragments, whereas the electron density of the LUMO and LUMO+1 were contributed significantly over the acceptor moiety of d orbitals of Cr^{3+} and also NO_3 group (Fig. S6). Additionally, the mapping of the frontier orbitals regarding the titled compounds associated with their energies are depicted in Fig. 11. As seen in Fig 11, in free ligand **P3** the electron contributions are localized over the almost whole molecule, except the phenyl ring attached to pyridine part. This result leads us to this fact that the coordination of Cr^{3+} with the **P3** and NO_3 moiety can be reinforced through electron donation of the coordinating oxygen atoms of ligand **P3** and moiety of the nitrate group and electron accepting of the nitrogen atom of phenylpyridine fragment.

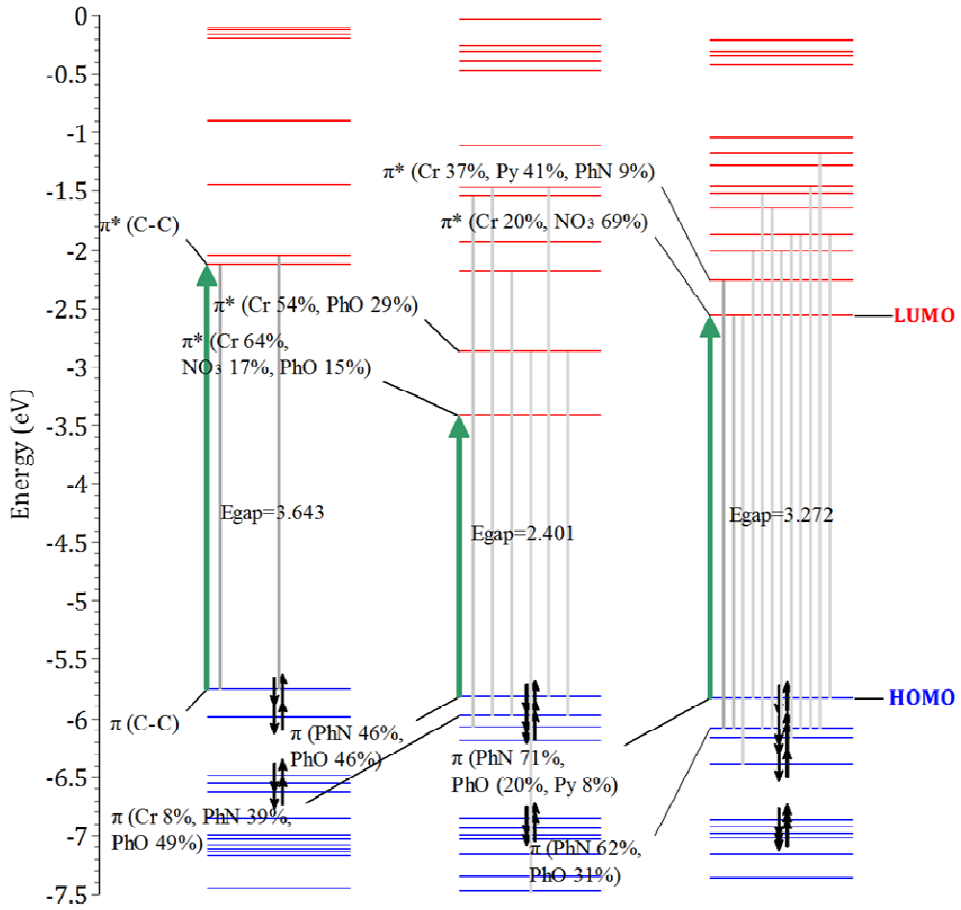

Fig. 10. The molecular orbital and some characters of HOMO and LUMO molecular orbitals of the (a) **P3**, (b) **P3**–Cr^{3+} (α-spin) and (c) **P3**–Cr^{3+} (β-spin) compounds.

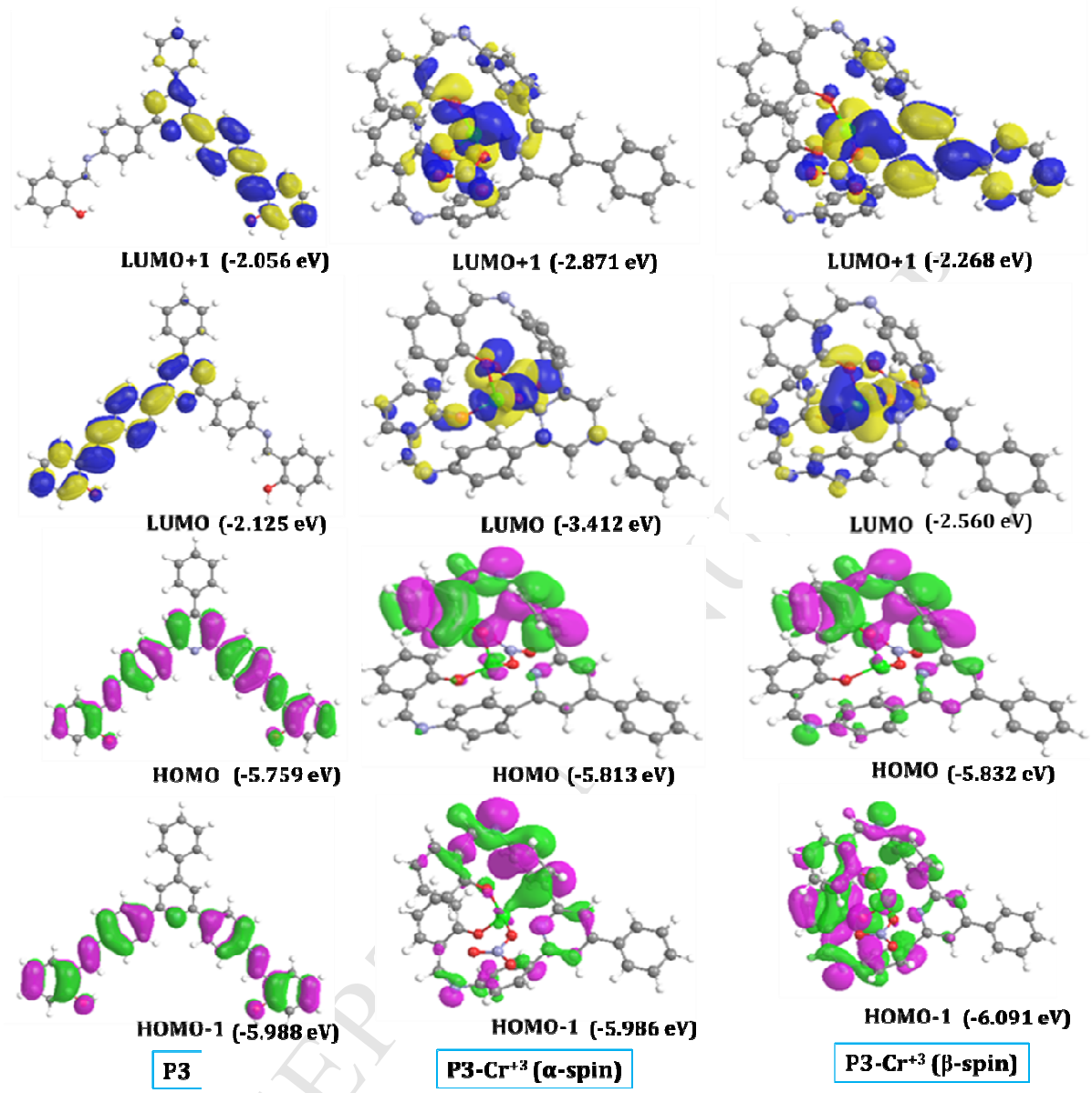

Fig. 11. Calculated the frontier molecular orbitals of the titled compounds with B3LYP/6-31G(d, p) level. Positive values of the HOMOs and LUMOs contour are represented in blue and purple and the negative values in yellow and green, respectively.

Figure 12 shows the UV-Vis spectra of both free ligand **P3** and its plausible tetrahedron complex **P3**–Cr^{3+}. The obtained UV-Vis spectra by means of TDDFT calculations are in good agreement with the experimental UV-Vis spectroscopy (Fig. S5). From the TDDFT calculations the exhibited band lines for **P3** showed at 311.7 nm (*f*=0.120), 318.2 nm (*f*=0.171), 355.5 nm (*f*=0.530), 367.9 nm (*f*=0.843), 385.0 nm (*f*=1.180) and for **P3**–Cr^{3+} complex revealed at 355.70

nm (*f*=0.010), 356.3 nm (*f*=0.011), 359.3 nm (*f*=0.014), 367.2 nm (*f*=0.007), 370.3 nm (*f*=0.008), 372.8 nm (*f*=0.006), 378.7 nm (*f*=0.008) and 380.4 nm (*f*=0.017), that are in agreement with the experimental spectrum. By complexation of the **P3** ligand to Cr^{3+} ion the intensity of the bands were decreased because of spin-forbidden transitions in 3d transition metals. The major transitions of the ligand **P3** at 367.9 nm and 385.0 nm are due the electron transition of (HOMO) → (LUMO) with dominant excitation characters of π-PhN (52%), π-PhO (27%) and π-Py (20%) to π^*-PhN (59%), π^*-PhO (23%) and π^*-Py (18%). The contributions on **P3** show that nitrogen lone pair electrons of Py fragment as belonging to HOMO is responsible for the fluorescence quenching. **P3**. On the other hand, the major lines for **P3**–Cr^{3+} at 367.2 nm are assigned to (HOMO-2) → (LUMO+2) associated with π-PhN (64%), π-PhO (25%) and π-Py (7%), d_x^2-$_y^2$-Cr (3%) to π^*-NO_3 (59%), d_{xy} -Cr (7%). As a result, the strong interaction between N atom of Py fragment and Cr^{3+} d-orbital causes to block the PET process from the nitrogen lone pair electron to the benzene, hence block the fluorescence quenching. The possibility of the restricted chelation-enhanced fluorescence (CHEF) process in **P3** coordinated to Cr^{3+} can be contributed the fluorescence enhancement along with the PET process [40].

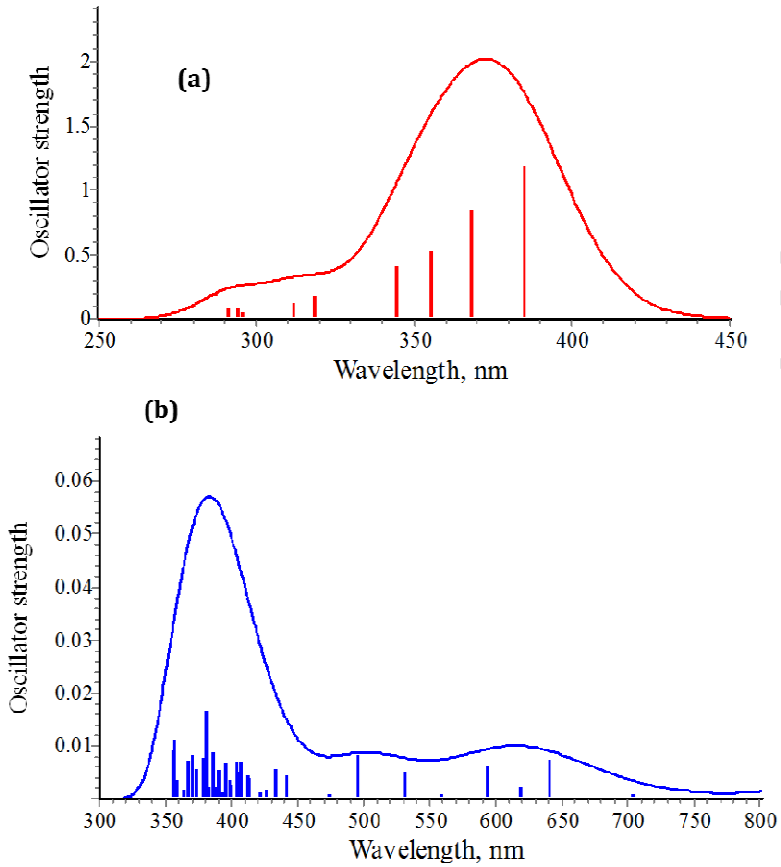

Fig. 12. The calculated UV-Vis spectra of the (a) **P3** and (b) **P3–Cr^{3+}** compounds.

3.8. Investigation of Binding reversibility

The reversibility **P3** binding with Cr^{3+} was evaluated by adding EDTA to **P3**–Cr^{3+} solution. It is assumed that the addition of EDTA will liberate Cr^{3+} from the **P3**–Cr^{3+} complex, releasing the **P3** ligand, because of the EDTA–Cr^{3+} complex (stability constant log $K_{EDTA–Cr}$ = 23.4) [53]. Therefore, 1 equiv. of EDTA (10 µM) was added to the Cr^{3+} (10 µM) complex of **P3** (10 µM) in CH_3CN/H_2O (95/5%) solution, exhibiting significant decrease of fluorescence signal at 663 nm. The addition of excess Cr^{3+} to the previous solution regenerates the fluorescence by participation of **P3** with another Cr^{3+} binding process (Fig. 13). The regenerated free **P3** can then participate in another Cr^{3+} binding process [54].

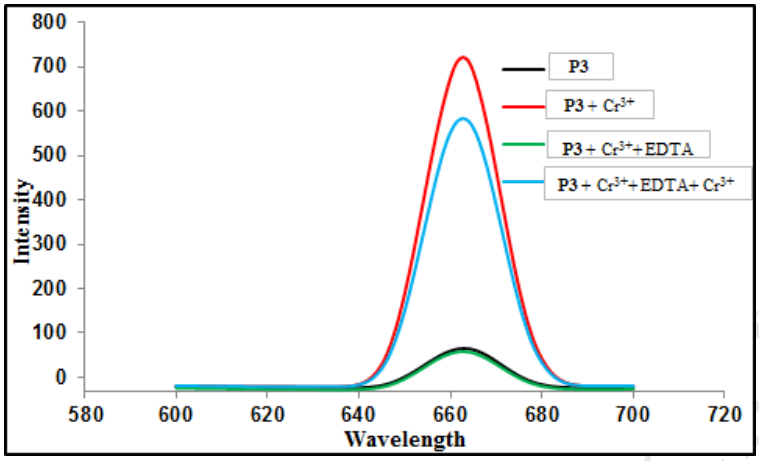

Fig. 13. Reversibility of Cr^{3+}–complex (10 µM) coordination to probe **P3** (10 µM) by EDTA (10 µM).

4. Conclusions

In summary, we have successfully developed a novel chemosensor **P3** which exhibited the high selectivity for Cr^{3+} in the presence of other metal ions. The sensor shows a large fluorescence enhancement in the presence of Cr^{3+} which is attributed to the interaction of **P3** and Cr^{3+} resulting in the efficient inhibition for the PET process. The results of Job's plot method together with theoretical study indicate that **P3** and Cr^{3+} form a 1:1 complex. The association constant K_a was determined to be 2.28×10^5 M^{-1} and the limit of detection (LOD) was calculated to be 1.3×10^{-7} M exhibiting more efficient than many other reported Cr^{3+} sensors. Besides, DFT calculations were carried out to get a comprehensive insight towards the plausible structure of **P3**–Cr^{3+} in the gas phase. The results confirmed tetrahedron geometry around the Cr^{+3} ions. In order to investigate the major excitation states and the absorption spectra of the compounds, TDDFT calculations were employed that were in agreement with the experimental results.

5. References

[1] C. Gou, S. H. Qin, H. Q. Wu, Y. Wang, J. Luo and X. Y. Liu, *Inorg. Chem. Commun.*, 2011, 14, 1622–1625.

[2] R. Azadbakht and H. Keypour, Spectrochim. Acta, part A., 2012, 85, 293–297.

[3] L. N. Wang, W. W. Qin and W. S. Liu, *Inorg. Chem. Commun.*, 2010, 13, 1122–1125.

[4] D. Udhayakumari, S. Saravanamoorthy, M. Ashok and S. Velmathi, *Tetrahedron Lett.*, 2011, 52, 4631–4635.

[5] A. Shafiee,,M.Z.Kassaee and A.R.Bekhradnia, *J. Heterocyclic Chem.,* 2007, 44, 471-474.

[6] C. M. Davis, K. H. Sumrall and J. B. Vincent, *Biochemistry.*, 1996, 35, 12963-12969.

[7] J. B. Vincent, *Nutr. Rev.*, 2000, 58, 67–72.

[8] C. Cervantes, J. Campos-García, S. Devars, F. Gutiérrez-Corona, H. Loza-Tavera and J. C. Torres-Guzmán, *FEMS Microbiol Rev*,. 2001, 25, 335-347.

[9] J. Mao, L. N. Wang, W. Dou, X. L. Tang, Y. Yan and W. S. Liu, *Org. Lett.*,2007, 9, 4567-4570.

[10] Z. G. Zhou, M. X. Yu, H. Yang, K. W. Huang, F. Y. Li and T. Yi, *Chem. Commun.*, 2008, 29, 3387-3389.

[11] K. Huang, H. Yang, Z. G Zhou, M. X Yu, F. Y Li and X. Gao, *Org. Lett*., 2008, 10, 2557-2560.

[12] A. J Weerasinghe, C. Schmiesing and E. Sinn, *Tetrahedron let.*, 2009, 50, 6407-6410.

[13] D. Wang, Y. Shiraishi and T. Hirai, *Tetrahedron Lett.*, 2010, 51, 2545-2549.

[14] X. Hu, X. Zhang, G. He, C. He and C. Duan, *Tetrahedron.*, 2011, 67, 1091-1095.

[15] Z. Li, L. Zhang, X. Li, Y. Guo, Z. Ni, J. Chen, L. Wei and M. Yu, *Dyes Pigments*,. 2012, 94, 60-65.

[16] M. Li, H. Y. Lu, R. L. Liu, J. D. Chen and C. F. Chen, *J. Org. Chem.*, 2012, 77, 3670-3673.

[17] E. Hao, T. Meng, M. Zhang, W. Pang, Y. Zhou and L. Jiao, *J. Phys. Chem. A*,. 2011, 115, 8234-8241.

[18] D. Ray and P. K. Bharadwaj, *Inorg. Chem.*, 2008, 47, 2252-2254.

[19] J. S. Wu, W. M. Liu, X. Q. Zhuang, F. Wang, P. F. Wang, S. L. Tao, X. H. Zhang, S. K. Wu and S. T. Lee, *Org. Lett.*, 2007, 9, 33-36.

[20] X. L. Tang, X. H. Peng, W. Dou, J. Mao, J. R. Zheng, W. W. Qin, W. S. Liu, J. Chang and X. J. Yao, *Org. Lett.*, 2008, 10, 3653-3656.

[21] B. Ramachandram, N. B. Sankaran, R. Karmakar, S. Saha and A. Samanta, *Tetrahedron.*, 2000, *56*, 7041-7044.

[22] V. B. Bojinov and T. N. Konstantinova, *Sens. Actuators B: Chem.*, 2007, 123, 869–876.

[23] V. B. Bojinov and I. P. Panova, *Dyes Pigments.*, 2009, 80, 61–66.

[24] V. B. Bojinov, N. I. Georgiev and P. S. Nikolov, *J. Photochem. Photobiol. A: Chem.*, 2008, 197, 281–289.

[25] V. B. Bojinova, I. P. Panovaa, D. B. Simeonovb and N. I. Georgieva, *J. Photochem. Photobiol. A: Chem.*, 2010, 210, 89–99.

[26] V. B. Bojinov, N. I. Georgiev and N. V. Marinova, *Sens. Actuators B: Chem.*, 2010, 148, 6–16.

[27] M. Sarkar, S. Banthia and A. Samanta, *Tetrahedron Lett.*, 2006, 47, 7575-7578

[28] B. Tamami and H. Yeganeh, *Polymer.*, 2001, 42, 415-420.

[29] M. J. Frisch, G. W. Trucks, H. B. Schlegel, G. E. Scuseria, M. A. Robb, J. R. Cheeseman, G. Scalmani, V. Barone, B. Mennucci, G. A. Petersson, H. Nakatsuji, M. Caricato, X. Li, H. P. Hratchian, A. F. Izmaylov, J. Bloino, G. Zheng, J. L. Sonnenberg, M. Hada, M. Ehara, K. Toyota, R. Fukuda, J. Hasegawa, M. Ishida, T. Nakajima, Y. Honda, O. Kitao, H. Nakai, T. Vreven, J. A. Montgomery Jr., J. E. Peralta, F. Ogliaro, M. Bearpark, J. J. Heyd, E. Brothers, K. N. Kudin, V. N. Staroverov, R. Kobayashi, J. Normand, K. Raghavachari, A. Rendell, J.C. Burant, S. S. Iyengar, J. Tomasi, M. Cossi, N. Rega, J. M. Millam, M. Klene, J. E. Knox, J. B. Cross, V. Bakken, C. Adamo, J. Jaramillo, R. Gomperts, R. E. Stratmann, O. Yazyev, A. J. Austin, R. Cammi, C. Pomelli, J. W. Ochterski, R. L. Martin, K. Morokuma, V. G. Zakrzewski, G. A. Voth, P. Salvador, J.J. Dannenberg, S. Dapprich, A.D. Daniels, O. Farkas, J.B. Foresman, J.V. Ortiz, J. Cioslowski, D. J. Fox, Gaussian 09, Revision A.1, Gaussian Inc, Wallingford, CT, 2009.

[30] C. Lee, W. Yang and R. G. Parr, *Phys. Rev.*, 1988, 37, 785–789.

[31] J. Tomasi, B. Mennucci and R. Cammi, *Chem. Rev.*, 2005, 105, 2999-3094.

[32] M. Z. Kassaee and A. R. Bekhradnia, *J. Biosci. Bioeng.*, 2003, 95, 526-529.

[33] N. C. Lim, S. V. Pavlova and C. Bruckner, *Inorg. Chem.*, 2009, 48, 1173-1182.

[34] P. Alaei, S. Rouhani, K. Gharanjiga and J. Ghasemi, *Spectrochim. Acta, Part A.*, 2012, 90, 85-89.

[35] R. M. F. Batista, S. P. G. Costa and M. M. M. Raposo, *J. Photochem. Photobiol. A: Chem.*, 2013, 259, 33-40.

[36] A. Bekhradnia, E. Domehri and M. Khosravi, *Spectrochim. Acta, Part A.*, 152 (2016) 18–22

[37] Z. Zhou, M. Yu, H. Yang, K. Huang, F. Li, T. Yi and C. Huang, *Chem. Commun.*, 29 (2008) 3387-3389.

[38] (a) C.A. Parker and W.T. Rees, *Analyst.*, 1960, 85, 587-600; (b) Y. Gabe, Y. Urano, K. Kikuchi, H. Kojima and T. Nagano, *J. Am. Chem. Soc.*, 2004, 126, 357-3367.

[39] S. Goswami, A. K. Das, A. K. Maity, A. Manna, K. S. AichMaity, P. Saha, T. K. Mandal, *Dalton Trans.*, 2014, 43, 231-239.

[40] G. B. Chalmardi, M. Tajbakhsh, A. Bekhradnia and R. Hosseinzadeh, *Inorg. Chim. Acta*., 2017, *462*, 241-248.

[41 J. R. Lakowicz, Principles of fluorescence spectroscopy, springer US. (2006).

[42] R. B. OrfãoJr, F. D. Carvalho, P. Homem-de-Mello and F. H. Bartoloni, *J. Braz. Chem. Soc.*, 2017, 28, 1896-1904.

[43] (a) Y. Yang, H. Xue, L. Chen, R. Sheng, X. Li and K. Li, *Chin. J. Chem.*, 2013, 31, 377-380; (b) J. Zhang, L. Zhang, Y. Wei, J. Chao, S. Wang, S. Shuang, Z. Cai and C. Dong, *Anal. Methods.*, 2013, 5, 5549-5554.

[44] P. Saluja, H. Sharma, N. Kaur, N. Singh and D. O. Jang, *Tetrahedron.*, 2012, 68, 2289–2293.

[45] L. K. Kumawat, N. Mergu, M. Asif and V. K. Gupta, *Sens. Actuators B:chem.*, 2016, 231, 847-859.

[46] Y. J. Jang, Y. H. Yeon, H. Y. Yang, J. Y. Noh, I. H. Hwang and C. Kim, *Inorg. Chem. Commun.*, 2013, 33, 48–51.

[47] W. Zhu, L. Yang, M. Fang, Z. Wu, Q. Zhang, F. Yin, Q. Huang and C. Li, *J. Lumin.*, 2015, 158, 38–43.

[48] S. Saha, P. Mahato, E. Suresh, A. Chakrabarty, M. Baidya, S. K. Ghosh and A. Das, *Inorg. Chem.*, 2011, 51, 336-345.

[49] N. Hasani and M. N. A. Al-Jibouri, *Res. Chem. Intermed.*, 2017, 43, 4585–4610.

[50] S.Arshadi, A.R. Bekhradnia and A. Ebrahimnejad, *Can. J. Chem*., 2011, 89, 1403–1409.

[51] S. M. Hossain, K. Singh, A. Lakma, R. N. Pradhan and A. K. Singh, *Sensors and Actuators B: Chemical*, 2017, 239, 1109-1117.

[52] E. Vessally, S. Soleimani-Amiri, A. Hosseinian, L. Edjlali and A. Bekhradnia, *Physica E*, 2017, 87, 308–311.

[53] D. Harvey, Modern Analytical Chemistry, McGraw-Hill Higher Education, 2000.

[54] (a) Y. S. Wu, C. Y. Li, Y. F. Li, J. L. Tang and D. Liu, *Sens. Actuators B: Chem.*,2014, *203*, 712-718 ; (b) Y. Long, J. Zhou, M.P. Yang and B.Q. Yang, *Chin. Chem. Lett.*, 2016, 27, 205–210.